Rare Metal Materials and Engineering
Volume 49, Issue 3, March 2020
Available online at www.rmme.ac.cn

Science Press

Cite this article as: Rare Metal Materials and Engineering, 2020, 49(3): 0811-0818.

ARTICLE

Effect of Rare Earth Ce on Microstructure and Wear Resistance of HMn64-8-5-1.5 Alloy

Chen Shaohua[1, 2], Mi Xujun[1], Bie Lifu[3], Huang Guojie[1]

[1] State Key Laboratory of Nonferrous Metals and Processes，General Research Institute for Nonferrous Metals (GRINM); GRIMAT Engineering Institute Co., Ltd; General Research Institute for Nonferrous Metals, Beijing 100088, China ;[2] Aluminum Corporation of China, Beijing 100082, China; [3] University of Shanghai for Science & Technology, Shanghai 200093, China

Abstract: The effect of rare earth Ce on microstructure and friction and wear properties of HMn64-8-5-1.5 alloy was studied. The results indicate that rare earth Ce plays the role of deoxidation, desulfurization, dehydrogenation and impurity removal during the smelting process, which can purify the alloy matrix and make the grain size remarkably refined. The friction and wear experiments show that the rare earth Ce can significantly improve the friction and wear properties of the material. When 0.2wt% Ce is added, the mass loss of the alloy is less than 25%. Wear mechanism of the alloy was analyzed by combining two kinds of friction and wear models. The major wear behavior of the alloy changes from adhesive wear to abrasive wear by adding 0.2 wt% Ce. The main reason for the change of wear mechanism of the alloy with and without the Ce addition is the effects of removing impurities and refining crystal grains caused by Ce, which increases the surface strength and ultimate deformation value of the alloy itself.

Key words: brass; rare earth; microstructure; wear resistance; wear mechanism

Synchronizer ring is a key component of the shifting operating system in automotive transmissions. Due to the high speed friction required during operation, the material should have excellent wear resistance[1,2]. Special brass is selected as the ideal car synchronizer ring material due to its high hardness, good wear resistance and low price[3,4]. However, in actual applications, the failure of the automobile synchronizer ring made of HMn64-8-5-1.5 special brass in the early stage (about 3,000 km) occurred from time to time, and it is found by analysis that the failure form is mainly surface wear[5]. In order to solve this problem, it is supposed to improve the wear resistance of HMn64-8-5-1.5 special brass by adjusting its composition to avoid the occurrence of the early failure of the synchronizer ring.

Rare earth elements can optimize the microstructure and properties of the alloy by hindering recrystallization, refining the grains and affecting the precipitation process. Zhang et al [6] reported that the addition of Nd can improve the microstructure of AM60 alloy. When adding 0.9 wt% Nd, AM60 alloy obtains the best performance. Hu et al[7] studied the effect of Sm on the microstructure and mechanical properties of AZ61 alloy and pointed that the AZ61 alloy showed the finest microstructure and the best mechanical properties when the Sm addition amount is 1wt%. Du et al[8,9] studied the effect of rare earth Ce on the as-cast microstructure and properties of aluminum alloy and found that 0.25 wt% Ce formed a new second phase in the alloy, which refined the matrix structure, and improved the wear resistance of the alloy. The results of Zhang et al [10] were consistent with the results of Ref.[8, 9]. Chaubey et al[11] studied the effect of Ce on the microstructure and properties of 7055Al alloy. It was found that when the Ce content increased from 0.1 wt% to 0.4 wt%, the dendritic structure was significantly refined. Wang et al[12] found that Ce could form GP zone and promote the formation of

Received date: March 29, 2019
Corresponding author: Mi Xujun, Ph. D., Professor, State Key Laboratory of Nonferrous Metals and Processes, General Research Institute for Nonferrous Metals (GRINM), Beijing 100088, P. R. China, E-mail: sklcopper1967@163.com

precipitated phase when studying the influence of Ce on the microstructure and properties of 2519Al alloy. Xiao et al[13] found that 0.45 wt% Ce could refine the precipitated phase in Al-Cu-Mg-Ag alloy and improve its thermal stability. Because of the complicated mechanism of rare earth in copper and its alloys, few research was carried out on the application of rare earth in copper and copper alloys. Based on the above beneficial effects of Ce on Al-Cu alloy, it is inferred that Ce may show the same effect on complex special brass.

In this study, rare earth Ce is added to HMn64-8-5-1.5 brass to investigate the effect of rare earth Ce on the pores, slags, purification and refinement of the matrix structure, friction and wear performances. The wear mechanism of special brass is also revealed at room temperature.

1 Experiment

HMn64-8-5-1.5 (Cu-19Zn8Mn-5.6Al-1.4Si-1.4Fe-0.7Pb) special brass alloy ingot, Cu-Ce (10 wt% Ce) alloy and electrolytic copper (99.95 wt%) were used as raw materials. ZG0025 medium frequency electromagnetic induction furnace and magnesium oxide crucible were used for melting and casting under atmospheric conditions. First, electrolytic copper and HMn64-8-5-1.5 alloy were mixed and melted, and then the Cu-Ce alloy was added to the molten alloy. The alloy was completely melted for 5 min and then poured into a cylindrical graphite mold with a diameter of 95 mm followed by air cooling. The chemical composition was measured by ICP (Inductive Coupled Plasma Emission Spectrometer) as shown in Table 1. The Ce content is 0.1 wt% and 0.2 wt% in the obtained samples.

The microstructures were observed by metallographic optical microscopy (OM) and scanning electron microscope (SEM). The crystal structures were analyzed by X-ray diffractometer (XRD), using Cu Kα radiation. The friction and wear properties were measured by the MMW-1A universal friction and wear tester. The pin-disc dry friction was carried out in the air for 30 min with the C45 steel as grinding ring material under the test load of 100 N and the rotation speed of 200 r/min. Each sample was tested for at least 3 times. Before and after each test, the samples were ultrasonically cleaned in acetone for 10 min followed by blown dry. The mass was measured by an electronic analytical balance with the minimum graduation value of 0.1 mg to calculate the mass loss. The thickness of the sample before and after wear test was measured by a spiral micrometer to calculate the depth of wear. The worn surfaces were characterized by SEM.

Table 1 Major element chemical composition of the experimental alloy (wt%)

Alloy	Zn	Mn	Al	Si	Fe	Pb	Ce	Cu
A1	19.08	8.00	5.62	1.40	1.42	0.72	0	Bal.
A2	19.05	8.02	5.44	1.48	1.40	0.72	0.1	Bal
A3	19.06	7.97	5.42	1.44	1.40	0.70	0.2	Bal.

Note: A1 is Ce-free, A2 and A3 is Ce-containing

2 Results and Discussion

2.1 Microstructure and XRD results

Fig.1 is XRD patterns of Ce-free (A1) and Ce-containing (A2 and A3) alloys. As shown in Fig.1a, A1, A2 and A3 alloys are mainly composed of β phase (rich in Cu, bcc crystal structure). The other peaks are smaller in intensity than the (100) peak and cannot be clearly observed. Therefore, a slower scanning speed of 0.16°/min was used from 43.5° to 50.0°. The diffraction peak of Mn_5Si_3 can be observed in Fig.1b, and it is believed that the Mn_5Si_3 phase forms in the A1, A2 and A3 alloys. Since Pb and Ce contents are low, the phase containing Pb and Ce is not detected.

The cross section metallographic structures of the A1, A2 and A3 alloys are shown in Fig.2. It can be seen from Fig.2 that the microstructure of the A1, A2 and A3 alloys is mainly composed of matrix β phase with Mn_5Si_3 particles, and the Mn_5Si_3 particle shows an irregular polygonal in cross section. The Mn_5Si_3 particles show various sizes in different areas. They are large in the grains, and the eutectic Mn_5Si_3 particles around the grain boundary are smaller. The

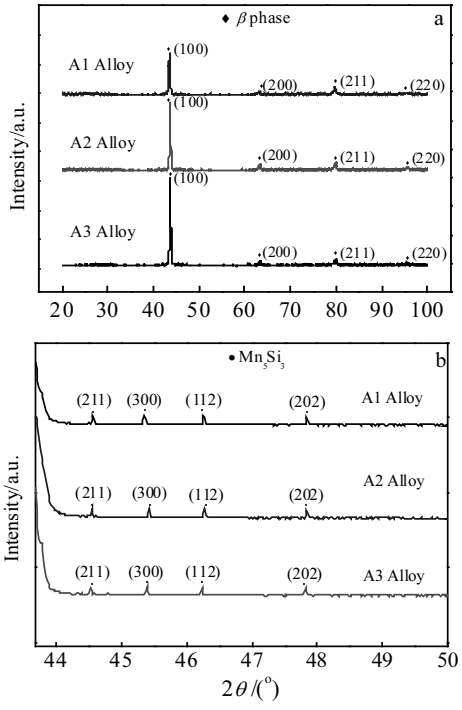

Fig.1 XRD patterns of A1, A2 and A3 alloys under different scanning speeds: (a) 2°/min and (b) 0.16°/min

grain size is remarkably refined by rare earth-doping by comparing A1, A2 and A3. The Mn_5Si_3 particle quantity is increased with the decrease of the size as the Ce content is increased from 0 wt% to 0.2 wt%.

Rare earth Ce can refine the grain of HMn64-8-5-1.5 alloy because Ce can react with some elements in the alloy to form high melting point compounds, which usually suspend as very fine particles during melting, become dispersed crystal nucleus, and make the crystal grains more and smaller during solidification[14,15]. Because the solubility of rare earth in copper alloys is small, it usually gathers at the front edge of the solid-liquid interface during solidification, which can promote the formation of new crystal nuclei and refine grains [16]. Since the atomic radius of rare earth Ce is larger than that of the atomic radius of Cu, Ce enters the crystal lattice of Cu to cause large lattice distortion, which increases the energy of the system. In order to maintain the lowest energy of the system, the Ce atom is enriched on the grain boundary with low density of the atom arrangement. Therefore, in the as-cast microstructure, rare earths mostly distribute in the grain boundaries and prevent grain growth. However, if excessive amount of rare earth is added, a large amount of rare earth compounds form and then reduce the supercooling effect of the rare earth atoms, which make the grains of the alloy coarsened[17].

2.2 Purification of rare earth Ce

Compared with A1 alloy, the addition of Ce eliminates the pores in the A2 alloy, reduces the inclusions between the grain boundaries, and improves the wear resistance of the alloy. This is because the rare earth Ce plays a good role in degassing and impurity removal. The related mechanism is as follows:

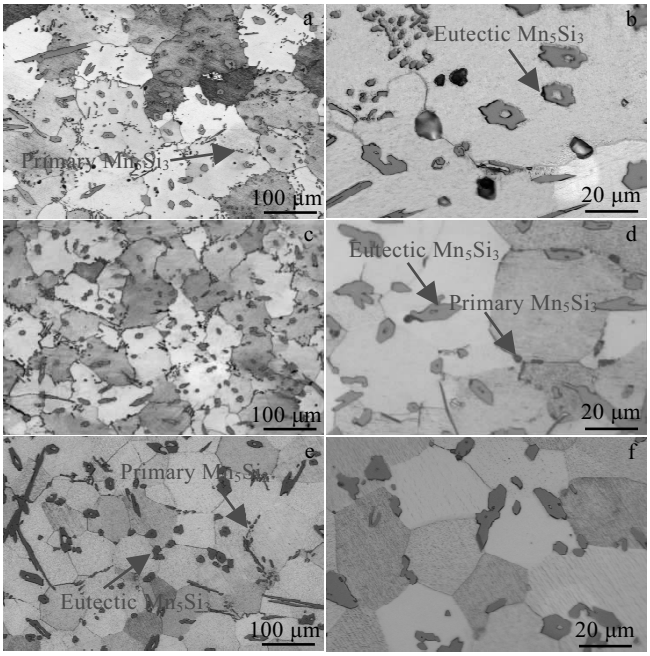

Fig.2 OM images of alloys: (a, b) A1, (c, d) A2, and (e, f) A3

2.2.1 Deoxidation

The outer electron arrangement of O is 1s22s22p4, which is not fully filled. O can absorb the outermost and subouter electrons of rare earth elements to form a more complex rare earth oxide. Therefore, the rare earth is a strong deoxidizer. After the deoxidation reaction is completed, the rare earth oxide will float on the surface of the copper liquid as solid phase, and the slag phase will be removed after cooling and solidification, so as to achieve the purpose of deoxidization.

The deoxidation reaction is as follows:

$$2[Ce]+3[O]=Ce_2O_3(s) \quad (1)$$

Standard reaction free energy at 1400 K is –58087 J/mol, deoxidation constant k=2.40×10^{-21}. The thermodynamics of deoxidation of rare earth Ce in copper is very strong, and it can remove almost all oxygen in the copper solution[18,19].

2.2.2 Desulfurization

The desulfurization principle of rare earth Ce in copper is consistent with the principle of deoxidation, which are as follows:

$$Cu_2S+Ce=2Cu+CeS \quad (2)$$

According to the thermodynamic data, it is calculated that the desulfurization reaction occurs above the melting point of copper, and the standard formation free enthalpy is related to temperature:

$$\Delta G_T^0 = -192360 + 9.2T\log T - 11.8T \quad (3)$$

Standard reaction free energy at 1400 K is –154950 J/mol. The equilibrium constant of the desulfurization reaction is k=3.16×10^{-6}. It is clear that in the copper liquid, the thermodynamic tendency of rare earth Ce desulfurization reaction is great, and rare earth Ce can remove a small amount of sulfur impurities in the copper[20].

2.2.3 Dehydrogenation

The dehydrogenation reaction of rare earth in copper solution can be typically described as the following process:

$$H_2 = 2[H]_{Cu} \quad (4)$$

$$RE+[H]_{Cu}=[REH]_{Solid\ solution} \quad (5)$$

$$[REH]_{Solid\ solution}+(x-1)[H]_{Cu}=REH_x \quad (6)$$

The REH_x types produced by the action of rare earth metals and hydrogen are REH2, REH3 and many non-integer hydride, which have a strong exothermic reaction. In copper processing, adding rare earth can quickly absorb hydrogen in atomic state from copper and produce hydride under certain conditions. The low density hydride easily float on the surface of the copper liquid and re-decompose at high temperatures causing hydrogen release[21].

2.2.4 Removal of miscellaneous

The element of Bi is mostly insoluble in copper. It is low melting point impurity in copper alloys and is harmful to the properties of copper alloys because it can produce low

melting point eutectic (Cu+Bi) with copper, which is distributed along the grain boundary. It is easy to cause cracking in hot rolling, which is so-called "thermal brittleness". Sulfur and oxygen and copper produce a melting point of about 1065 ºC (Cu+Cu_2S) and (Cu+Cu_2O) eutectic brittle phase, affecting the processing performance of the alloy. Rare earth elements are chemically activated and can form refractory binary or multi-component compounds with many fusible components. These compounds have higher melting points and lower density than copper, and thus it is easy to float and can eliminate harmful impurities at grain boundaries. Owning to the purification effect of rare earth, the conductivity, thermal conductivity and process ability of copper are improved. However, after exceeding the appropriate range, the compound precipitates formed by rare earth elements themselves and other elements also become inclusions, then making the performance deterioration[22,23].

Table 2 shows the contents of O, H, S and Bi in A1, A2 and A3 alloys. With the addition of rare earth element Ce, the slags in alloys gradually are decreased.

Metallographic photographs and TEM images of the A1 and A3 alloy samples are shown in Fig.3. There are defects such as pores and slags around the grain boundaries. The A1 alloy without Ce shows more pores and slags, while the pores in the A3 alloy with 0.2 wt% Ce are basically eliminated with the decrease of the slags. The TEM analysis shows that the grain boundaries are purified by adding rare earth Ce, as shown in Fig.3c and Fig.3d.

Table 2 Impurity element chemical composition of the experimental alloy (wt%)

Alloy	Ce	O	S	H	Bi
A1	0	40	18	10	100
A2	0.1	32	13	8	60
A3	0.2	25	11	7	50

Note: A1 is Ce-free, A2 and A3 is Ce-containing

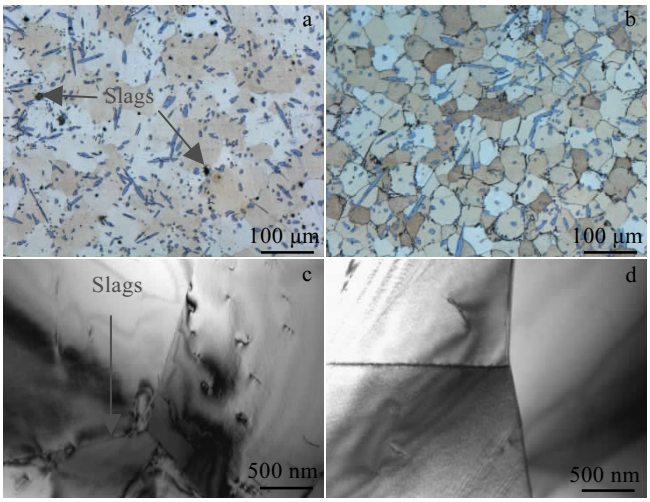

Fig.3 OM images (a, b) and TEM images of (c, d) alloys: (a, c) A1 and (b, d) A3

2.3 Friction performance

The friction coefficient and mass loss of the A1, A2 and A3 alloy samples were measured and analyzed. As shown in Fig.4 and Fig.5, when the Ce content is 0 wt%, the average wear coefficient of the A1 alloy sample is 0.405, the mass loss is 47.9 mg, and the wear depth is 92.6 μm. The wear properties of A2 are between those of A1 and A3. The average friction coefficient is 0.365, the mass loss is 40.2 mg, and the wear depth is 86 μm. The average friction coefficient of the A3 alloy sample with Ce content of 0.2 wt% is 0.312, the mass loss is reduced to 35.5 mg, and the wear depth is 67.8 μm. In addition, the friction coefficient of A1 alloy fluctuates largely, indicating that the friction process is unstable. The friction coefficient of A3 alloy is flat, indicating that the friction process is more stable than that of A1 alloy. It indicates that the wear resistance of HMn64-8-5-1.5 alloy is significantly improved by the addition of rare earth Ce.

2.4 Friction model

The essence of material wear is the complex physical and chemical reactions occurring between the friction interfaces, which includes the external elastic force to cause elastoplastic deformation of the material, the change of interface energy caused by the deformation heat of the

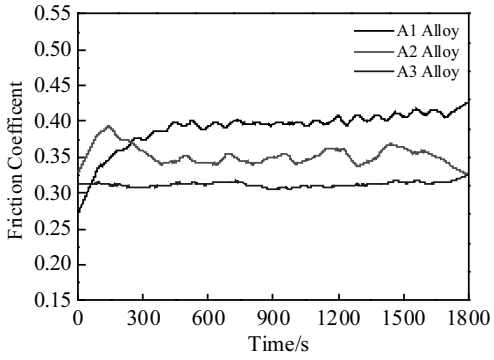

Fig.4 Friction coefficient of A1, A2 and A3 Alloy

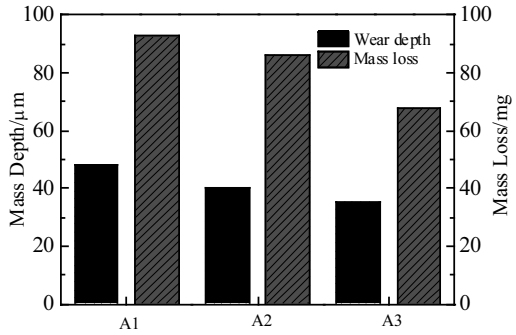

Fig.5 Wear volume and wear depth of A1, A2 and A3 Alloy

contact zone, the transfer or shedding of the material caused by the transformation of the interface energy, the material type or property transformation, etc.

2.4.1 Adhesive wear of A1 alloy

When adhesive wear occurs between the metals, the metal with weak surface strength will produce partial shedding. As the friction process continues, the shedding material will gradually transfer to the metal surface with strong surface strength. The transfer process is shown in Fig.6. The strong adhesion between metals can be explained by the electron transfer mechanism between the contacting surfaces. There are many free electrons between the metals. When the two metals contact, the free electrons between the two contacting surfaces can transfer to each other to form a bond. In order to explain the bonding growth mechanism between the contact faces, it is assumed that there is a certain load on the contact surface. The load strength is greater than the surface yield strength of the material and is sufficient to cause plastic deformation at the contact point. Due to the plastic deformation at the contact point, the flow deformation produces shear stress, and the material is under the action of shear stress. The actual contact area is gradually increased, and the increase of contact area will result in the decrease of normal pressure and allow the material surface to withstand greater shear stress. Therefore, the shear stress and the actual contact area continue to increase until the yield strength of the material itself is reached.

The bond growth mechanism between the contact surfaces could be described by considering the Von Mises yield model[24]. In this model, the material will plastically deform under the following conditions:

$$P^2 + 3\tau^2 = P_y^2 \quad (7)$$

Where, P is the normal contact stress (pressure) (Pa), τ is the effective shear stress (Pa) at the time of contact, and P_y is the plastic flow stress (yield strength) (Pa) of the material.

Since the yield strength at the contact point is affected by contact stress P and shear stress τ, a similar descriptive formula is proposed:

$$P^2 + C\tau^2 = P_0^2 \quad (8)$$

Where, C is a constant with a hypothetical value close to 10, P_0 is the plastic flow stress (Pa) of the material without tangential forces.

From Formula (8), it can be known that if the normal load only acts on the Contact Point τ=0,

Then: P=P_0

In addition, P, τ, P_0 can be expressed as follows:

$$P = \frac{W}{A_r} \quad \tau = \frac{F}{A_r} \quad P_0 = \frac{W}{A_{ro}} \quad (9)$$

Where, F is the frictional force, W is the normal load (N), A_r is the true contact area (m^2) when the surface has a tangential force. A_{r0} is the true contact area (m^2) when the surface does not have a tangential force.

Take these expressions into equation (8):

$$(W/A_r)^2 + C(F/A_r)^2 = (W/A_{ro})^2 \quad (10)$$

$$\frac{A_r}{A_{ro}} = [1 + C\frac{F^2}{W^2}]^{0.5} \quad (11)$$

It can be seen from Formula (11) that increasing the tangential force will increase the actual contact area, and thus the adhesion will be increased. According to Fig.2a~2b, there are many pores and defects in A1 alloy without adding rare earth Ce. The presence of pores and defects reduces the surface strength of the alloy, increases the plugging of dislocations, and increases the surface shear stress, and then the adhesion increases. The addition of rare earth Ce results in the degassing and impurities removal and grain refining, makes the material denser, reduces dislocation plugging, and thus decreases the adhesion tendency.

Fig.7 shows the wear surface morphologies of A1 alloy. According to Fig.7, the wear mechanism of the A1 alloy sample is mainly adhesive wear, and the wear surface of the A1 alloy is very rough and a large amount of plastic deformation is generated. Under the action of shear stress, the stress on the surface of alloy accumulates continuously, and plastic deformation occurs in the stress concentration zone. The region where the plastic deformation occurs is torn under the further action of the shear stress until a pit is formed away from the surface of the substrate. In addition, during the friction process, the surface particles of the alloy are continuously transferred to the surface of the other pair of friction pairs. Under the cyclic frictional conditions, the transferred particles gradually accumulate on the surface of the friction pair.

After accumulating to a certain extent, the abrasive granules are generated and peeled off due to fatigue fracture

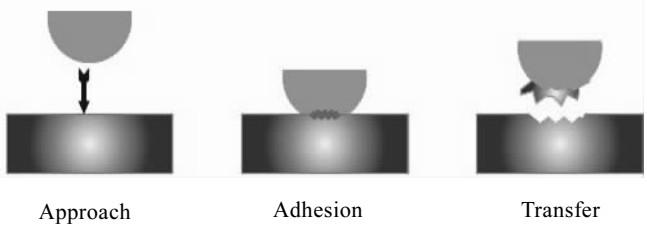

Fig.6 Adhesive wear model for a single bond point

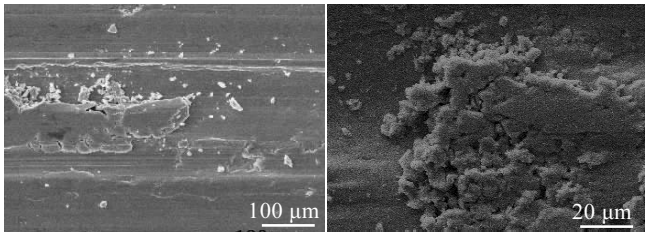

Fig.7 SEM images of worn surfaces of A1

or bond chain destruction, and the detached abrasive chips are further combined with the alloy surface and grown to form a transfer layer[19,25]. This is consistent with the A1 alloy friction model analysis.

2.4.2 Abrasive wear of A3 alloy

The friction process is actually the relative sliding of the microprotrusions on the material surface and the grinding pair surface[26]. Fig.8 is the basic model of abrasive wear. In this model, the microprotrusions are assumed to be tapered hard particles and all the abrasive grains are the same. Under the applied load, the abrasive grains are pressed into the softer material to form a groove by reciprocating motion.

The single abrasive load is the product of the cone indentation area and the yield stress (hardness) of the material under the indentation.

$$W_g = 0.5\pi(d\cot\alpha)^2 H \quad (12)$$

Where, W_g is the load on a single abrasive grain, d is the depth of the indentation, α is the angle of inclination of the cone particle, and H is the yield stress (hardness) of the material under the indentation.

The approximate volume of material removed by the cone particles is the product of the indentation cross-sectional area $d^2\cot\alpha$ and the particle moving distance l:

$$V_g = ld^2\cot\alpha \quad (13)$$

Where, V_g is the volume of material removed by the cone particles, l is the moving distance of the cone particles.

Substituting d in Eq.(12) into Eq.(13) yields an expression of the material wear volume expressed by load, abrasive shape, and sliding distance:

$$V_g = \frac{2l\tan\alpha}{\pi H}\cdot W_g \quad (14)$$

The total wear of the material is the sum of the individual abrasive wear:

$$V_t = \sum V_g = \frac{2l\tan\alpha}{\pi H}\cdot\sum W_g = \frac{2l\tan\alpha}{\pi H}\cdot W_t \quad (15)$$

Where, V_g is the total wear volume, W_t is the total load.

It is worth noting that the Formula (15) is established on the assumption that each cone particle is displaced and all materials are completely removed. That means the formula is suitable for the ideal "cutting" mechanism of abrasive wear. However, in practice, particles do not produce a certain plastic deformation on the surface. Therefore, Formula (15) is usually used to calculate the abrasive wear rate, which is the ratio of the real wear amount to the ideal calculation of the wear amount.

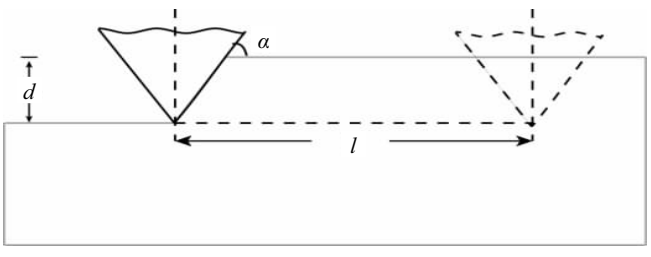

Fig.8 Basic model of abrasive wear of individual particles

Fig.9 shows that the wear pattern of A2 and A3 alloy is mainly abrasive wear after the addition of rare earth Ce. Compared with A1 alloy (Fig.7), the groove of A3 alloy wear surface becomes shallower and the shape deformation area decreases. The addition of rare earth Ce refines the alloy (Fig.2) and makes the alloy structure more uniform and denser, and thus frictional shear stress is more difficult to plastically deform on the surface of the alloy. These factors are beneficial to enhance the friction resistance of the alloy.

As shown in Fig.7 and Fig.9, the scratches on both sides of the worn surface of each sample produce different degrees of plastic deformation. The worn surface of A1 alloy produces a relatively obvious deformation, but there are just a small amount of plastic deformation on the worn surface of A3 alloy. Therefore, a finer and more accurate abrasive wear model is developed for better applicability.

In this model, it is considered that during abrasive wear, the material will not be simply worn by particles and disappear from the surface to form a groove, but that most of the worn material is moved to the side of the groove. If the material is extensible, the worn material is deformed and kept at the edge of the groove in the form of a “barrier”, as shown in the parts A_1, A_2 of Fig.10.

The model introduces a new parameter, defined as the ratio of the amount of material worn by the hard particles from the surface to the volume of the groove, that is:

$$f_{ab} = 1 - \frac{A_1 + A_2}{A_V} \quad (16)$$

Where, f_{ab} is the ratio of the amount of material removed by the gravel to the volume of the wear groove (f_{ab}=1 indicates

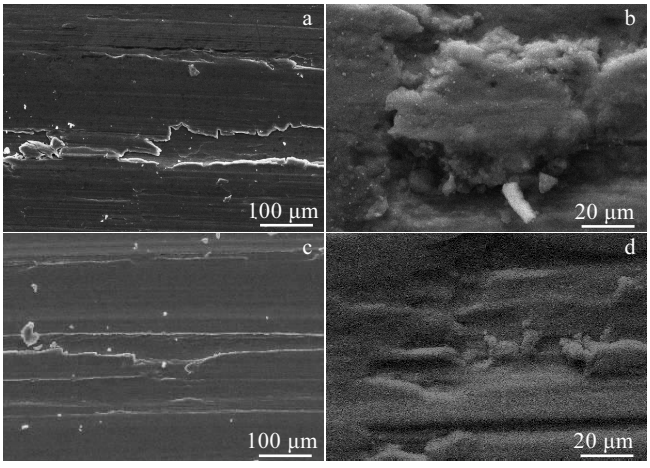

Fig.9 SEM images of worn surfaces of alloys: (a, b) A2 and (c, d) A3

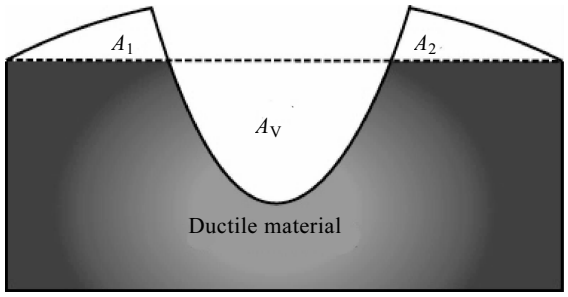

Fig.10 Material removal and displacement model in ductile abrasive wear

the ideal cutting mechanism, f_{ab}=0 indicates the ideal fatigue mechanism, and f_{ab}>1 indicates the crack mechanism), A_V is the wear groove cross-sectional area, (A_1+A_2) is the material "barrier" cross-sectional area deformed at the edges of both sides of the groove.

When the displacement is "1", the corresponding unit volume wear is:

$$\Delta V_l = \frac{\Delta V}{l} = f_{ab} A_V \tag{17}$$

Where, ΔV is the amount of wear per unit volume.

$$\Delta V_{d,\ ductile} = \frac{\Delta V}{lA} = f_{ab} \frac{A_V}{A} \tag{18}$$

Where, ΔV_d is the linear wear rate or wear depth of the unit sliding distance, and A is the macro contact area. For example, the macro contact area in the pin-disc friction experiment is the contact area of the pin and the disk.

The ratio of the actual contact area to the macro contact area in contact with the abrasive particles is:

$$\frac{A_V}{A} = \frac{\Phi_1 P}{H_{def}} \tag{19}$$

Where, Φ_1 is the coefficient depending on the shape of the abrasive particles, P is the externally applied pressure, and H_{def} is the hardness when the material is deformed.

For malleable materials, the parameter f_{ab} under wear and tear condition is closely related to the effective deformation on the wear surface and the ultimate deformation of the material, which can be referred to the principle of plasticity:

$$f_{ab} = 1 - (\varphi_{lim} / \varphi_s)^{2/\beta} \tag{20}$$

Where, φ_{lim} is the ultimate deformation value in the abrasive wear system, the maximum plastic deformation allowed by the material, φ_s is the effective plastic deformation on the wear surface, and β is a coefficient that describes deformation or strain decline when the depth is below the surface, which is mainly affected by the processing hardening behavior of the worn material and is usually β=1.

According to the Formula (20), the value of the parameter fab is closely related to the characteristics of the material itself, and also depends on the characteristics of the abrasive grains, such as the shape of the abrasive grains, the hardness of the particles. The addition of rare earth Ce achieves the function of degassing and removing impurities and refining grains. These factors will change the ultimate deformation value of the alloy itself and lead to the change of f_{ab} value. Therefore, the wear resistance of A3 alloy is higher than that of A1 alloy.

3 Conclusions

1) HMn64-8-5-1.5 alloy is mainly composed of matrix β phase with Mn_5Si_3 particle. The Mn_5Si_3 particle phase shows quite different morphologies in the same sample. The particle distributing inside the matrix grains is large, while the eutectic Mn_5Si_3 particle distributing at the grain boundary is small in size.

2) The addition of Ce promotes the nucleation of β phase matrix, and refines the grain size. At the same time, Ce plays a good role in degassing and impurity removal, and purifies the microstructure of the matrix.

3) The wear resistance of HMn64-8-5-1.5 alloy is significantly improved due to the refinement of the grain, degasification and hybridization of the Ce.

4) The friction model of HMn64-8-5-1.5 alloy is established. It is found that the wear mechanism of HMn64-8-5-1.5 alloy without Ce is adhesive wear, while the wear mechanism of HMn64-8-5-1.5 alloy with 0.2Ce is mainly abrasive wear.

References

1 Ismail K M, Elsherif R M, Badawy W A. *Electrochimica Acta*[J], 2004, 49(28): 5151
2 Lus H M, Ozer G, Guler K A *et al*. *International Journal of Cast Metals Research*[J], 2015, 28(1): 59
3 Li Q L, Xia T D, Lan Y F *et al*. *Applied Mechanics & Materials* [J], 2014, 490-491: 83
4 Antonijević M M, Milić S M, Šerbula S M *et al*. *Electrochimica Acta*[J], 2005, 50(18): 3693
5 Liu W G. *Auto &Vehicles*[J], 2016, 7(2): 67
6 Zhang J, Wang S, Zhang J *et al*. *Rare Metal Materials & Engineering*[J], 2009, 38(7): 1141
7 Hu Z, Hua Q, Yan H *et al*. *Rare Metal Materials & Engineering*[J], 2016, 45(9): 2275
8 Du J D, Ding D Y, Xu Z *et al*. *Materials Characterization*[J], 2017, 123: 42
9 Du J D, Ding D Y, Zhang W L *et al*. *Applied Surface Science*[J], 2017, 422: 221
10 Zhang J C, Ding D Y, Xu X L *et al*. *Journal of Alloys and Compounds*[J], 2014, 617: 665
11 Chaubey A K, Mohapatra S, Jayasankar K *et al*. *Transactions*

of the Indian Institute of Metals[J], 2009, 62(6): 539
12 Wang W T, Zhang X M, Gao Z G *et al. Journal of Alloys & Compounds*[J], 2010, 491(1-2): 366
13 Xiao D H, Wang J N, Ding D Y *et al*. *Journal of Alloys and Compounds*[J], 2003, 352: 84
14 Zhang Junchao, Ding Dongyan, Zhang Wenlong *et al. Nonferrous Metal Materials & Engineering*[J], 2016, 37(3): 78 (in Chinses)
15 Wang C, Zhu W, Peng A *et al*. *Environment International*[J], 2001, 26(5-6): 309
16 Mao X Y, Fang F, Tan R S *et al*. *Chinese Rare Earths*[J], 2008, 29(3): 75 (in Chinses)
17 Wang Z W, Chen S H, Li Y F *et al*. *Materials Science Forum*[J], 2016, 852: 472
18 Pola A, Montesano L, Gelfi M *et al. Wear*[J], 2016, 368-369: 445
19 Zhou K C, Xiao J K, Zhang L *et al*. *Wear*[J], 2015, 326-327: 48
20 Du T. *Acta Metallurgica Sinica*[J], 1997, 33(1): 69
21 Du T. *Transactions of Nonferrous Metals Society of China*[J], 1996, 6(2): 13
22 Wang M, Hong Z, Lin W. *Journal of Rare Earths*[J], 2007, 25(2): 233
23 Qinglin L I, Xia T, Lan Y *et al*. *Journal of Alloys and Compounds*[J], 2013, 562(1): 25
24 Lemaitre J, Desmorat R. *Engineering Damage Mechanics*[M]. Paris: Springer, 2005
25 Amirat M, Zaïdi H, Djamaï A *et al*. *Wear*[J], 2009, 267(1-4): 433
26 Bowden F P, Tabor D. *American Journal of Physics*[M]. Oxford: Clarendon Press, 1986: 292

稀土 Ce 对 HMn64-8-5-1.5 合金组织及耐磨性能的影响

陈少华[1,2]，米绪军[1]，别立夫[3]，黄国杰[1]

(1. 有研科技集团有限公司 有色金属材料制备加工国家重点实验室 有研工程技术研究院有限公司
北京有色金属研究总院，北京 100088)

(2. 中国铝业集团有限公司，北京 100082)

(3. 上海理工大学，上海 200093)

摘　要：研究了稀土 Ce 对 HMn64-8-5-1.5 合金显微组织及摩擦磨损性能的影响。研究表明，稀土 Ce 在熔炼过程中起到脱氧、脱硫、除氢和除杂的作用，可以净化合金基体，使晶粒尺寸显著细化。摩擦磨损实验表明，稀土 Ce 能明显改善材料的摩擦磨损性能，添加 0.2%Ce (质量分数)时，较无 Ce 的合金磨损量减小了 25%。添加 0.2%Ce 后，合金的主要磨损形式从严重的黏着磨损转变为磨粒磨损。结合 2 种摩擦磨损模型对合金的磨损机理进行了深入分析，添加稀土 Ce 前后合金的磨损机制发生变化的主要原因是稀土 Ce 能去除杂质、细化晶粒的作用，使合金本身的表面强度、极限变形值增大。

关键词：黄铜；稀土；显微组织；耐磨性能；磨损机理

作者简介：陈少华，女，1972 年生，博士，教授级高工，北京有研工程技术研究院有限公司，有色金属材料制备加工国家重点实验室，北京 100088，电话：010-82298950，E-mail: shh_chen@chalco.com.cn